aerospace

MDPI

Article

Experimental Study of a Planar Solid-Propellant Pulsed Plasma Thruster Using Graphite

Merlan Dosbolayev [1], Zhanbolat Igibayev [1,*] and Ongdassyn Yertayev [2]

[1] Institute of Experimental and Theoretical Physics, Al-Farabi Kazakh National University, Almaty 050040, Kazakhstan; merlan@physics.kz
[2] National Nanotechnology Open Laboratory, Al-Farabi Kazakh National University, Almaty 050040, Kazakhstan; ondas_83@mail.ru
* Correspondence: igizhan09@gmail.com

Abstract

The study presents an upgraded design and the results of experimental investigations of a solid-propellant pulsed plasma thruster (PPT) in which graphite simultaneously serves as both the propellant and the ignition element. The proposed configuration comprises a planar parallel system of copper electrodes and a graphite initiating electrode equipped with an electromagnetic discharge-triggering mechanism. Experimental tests were conducted under vacuum conditions of approximately 10^{-5} Torr at an energy-storage capacitor voltage of 800–1400 V. Discharge current amplitudes of up to 3.16 kA were recorded at a single-pulse energy of up to 4.41 J. The measured impulse bit was about 17.1 μN ·s, and the plasma jet exhaust velocity reached 11.1 km/s. Spectroscopic analysis of the plasma confirmed the presence of characteristic carbon emission lines, thereby indicating the active participation of the graphite propellant in the formation of the plasma plume. The present work continues previous research on PPTs with graphite electrodes and is aimed at further miniaturization of the earlier developed design. The primary objective of the study is the experimental validation of the proposed discharge concept in a planar parallel electrode configuration while preserving the key thrust and energy performance characteristics of the thruster.

Keywords: pulsed plasma thruster; solid propellant; graphite; vacuum testing; spectroscopy; small spacecraft; impulse bit

1. Introduction

The growing deployment of small spacecraft (SSC) has generated increasing demand for compact, reliable, and cost-effective propulsion systems capable of producing microthrust [1]. In this context, PPTs are considered one of the most promising solutions. Their key advantages—simple design, high specific impulse, and the ability to operate on solid propellant—eliminate the need for complex propellant storage and feed systems [2,3].

An important operational feature of PPTs is their capability to generate precise low-thrust levels by adjusting the pulse repetition frequency and duty cycle, which enables highly accurate control of the cumulative velocity impulse [4]. This advantage, together with low power consumption, has been demonstrated in studies of specific PPT implementations such as the Micro-Cathode Arc Thruster [5]. The ability of PPTs to deliver accurately controlled impulse bits is further supported by the experimental work of Zhang et al. (2022), where these thrusters exhibit high repeatability and predictability of single-pulse thrust-an essential requirement for orbital maneuvering and fine attitude control of

Check for updates

Academic Editor: Yanfang Liu

Received: 4 December 2025
Revised: 26 December 2025
Accepted: 6 January 2026
Published: 8 January 2026

Copyright: © 2026 by the authors. Licensee MDPI, Basel, Switzerland. This article is an open access article distributed under the terms and conditions of the Creative Commons Attribution (CC BY) license.

SSCs [6]. The planar parallel configuration of the thruster ensures a more uniform electric-field distribution and contributes to the formation of a stable plasma channel [7]. The use of graphite as both propellant and expendable igniting electrode offers several advantages, including a high sublimation temperature, good electrical conductivity, and stable ablation characteristics [8]. These properties make graphite a promising material for long-term operation under repeated pulsed discharges. Thus, the combination of the aforementioned advantages—simplicity, low cost, solid-propellant operation, precise impulse control, and modest power requirements—makes PPTs a highly attractive propulsion option for SSC applications [9].

A distinctive feature of the proposed planar parallel PPT design is the incorporation of an electromagnetic ignition mechanism that drives the graphite core into contact with the common electrode—the cathode—upon application of a control pulse. This initiates a spark breakdown followed by the formation of the main plasma discharge. Such a configuration improves operational stability, simplifies ignition, and eliminates the need for a separate triggering system. This study continues earlier developments [10,11], including a PPT model employing graphite as the propellant, and introduces several enhancements aimed at improving the thruster's performance and operational characteristics. Previous experiments employed coaxial configurations with relatively large electrode dimensions, which limited the potential for miniaturization and integration of the thruster into small satellite platforms. In the present work, a planar parallel electrode arrangement is implemented, offering a more compact architecture while maintaining discharge stability and the key thrust characteristics.

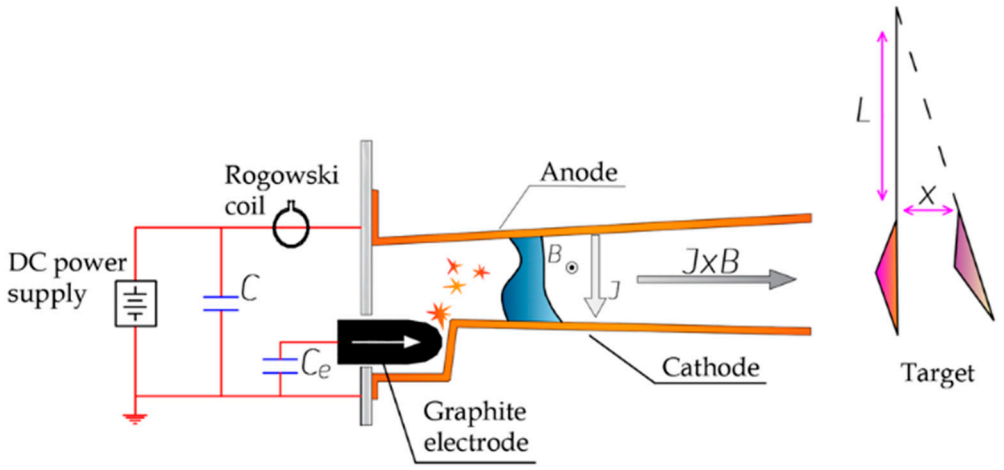
The manuscript is organized as follows. The Section 1 presents the main objectives and the relevance of the study. The Section 2 describes the thruster design, its operating principle, main parameters, and the experimental methods used. The Section 3 includes subsections on discharge current measurement, spectral analysis, high-speed imaging of plasma jet dynamics, and impulse bit measurements using a ballistic pendulum. The Section 4 summarizes the main findings and provides recommendations for future work.

2. Design Features of the Thruster and Experimental Methodology

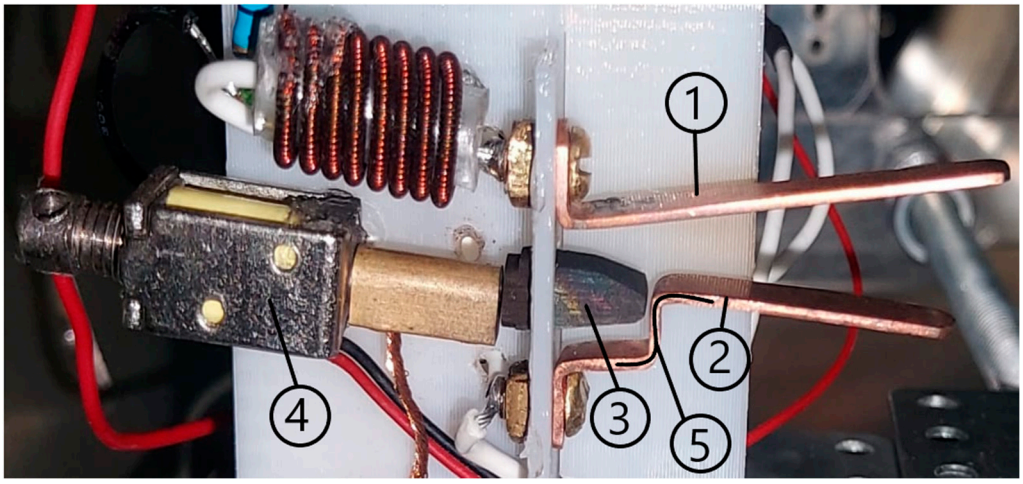
PPTs are electric propulsion devices in which electrical energy is converted into the kinetic energy of weakly ionized plasma. The operation of the thruster is based on the acceleration of charged particles in the electromagnetic field generated during a short high-voltage discharge between the electrodes. The primary parameters determining PPT performance include the specific impulse, single-pulse energy, propellant consumption, and ignition stability [2,12,13].

The discharge is initiated as follows: When a control pulse is applied, the graphite core, driven by the electromagnet, briefly closes the interelectrode gap by making contact with the cathode. This interaction produces a spark breakdown, leading to the formation of the main discharge current between the planar parallel electrodes. The resulting discharge current ionizes graphite particles and vapor, forming a plasma column that is subsequently accelerated by Lorentz forces within the discharge channel [14]. The absence of a stationary external ignition source simplifies the design and enhances reliability by reducing the number of potential failure points.

Figure 1 shows the schematic diagram (a) and a photograph (b) of the modified PPT. The thruster consists of a planar copper anode (1) and cathode (2), each with dimensions of $30 \times 5 \times 0.9$ mm. The cathode includes a bent section (5) housing the ignition electrode, which is a graphite electrode (3) with dimensions of $4 \times 4 \times 10$ mm. Table 1 summarizes the experimental parameters used in the study under variations in the input control signal.



(**a**)



(**b**)

Figure 1. (**a**) Schematic diagram of the experimental setup; (**b**) photo of the PPT (1—anode, 2—cathode, 3—igniting graphite electrode, 4—electromagnetic actuation mechanism, 5—bent section of the cathode).

Table 1. Main nominal parameters of the PPT.

Initial voltage (kV)	0.8–1.5
Discharge current (kA)	1.68–3.16
Pulse duration (μs)	6
Capacitance (μF)	4.5
Ignition voltage (V)	70
Length of the electrode (mm)	30
Width of the electrode (mm)	5
Cathode and anode material	Copper
Ignition electrode-propellant	Graphite

This geometry ensures a compact configuration and a stable discharge initiation zone. A distinctive feature of the thruster is the integrated electromagnetic ignition mechanism (4) located at the rear of the housing, as shown in Figure 1b. When a 5 V control pulse is applied, the electromagnet actuates the graphite core (3), bringing it briefly into contact with the cathode and initiating a spark breakdown. This enables discharge initiation without the need for a high-voltage stationary external ignition system. The main discharge circuit includes a capacitor with a capacitance of 4.5 μF (C), charged to 800–1500 V. A

supplementary circuit with a 22 μF capacitor (C_e) charged to 100 V is employed to generate the preliminary spark discharge. These parameters ensure reliable and repeatable ignition of the propellant at each activation.

The discharge current is recorded using a 500-turn Rogowski coil (Figure 1a) with an outer diameter of 9.2 mm. The coil is connected to an RC integrator, while the charging voltage is monitored using a PINTECH P6008 high-voltage probe (Guangzhou Pintech Co., Ltd., Guangzhou, China).

To determine the elemental composition and study the dynamics of the plasma jet, an ATL 30,007 broadband spectrometer (Optosky Photonics Inc., Xiamen, China)) and a high-speed Phantom v2512 CMOS (Vision Research Inc., Wayne, NJ, USA) camera were used, respectively. All experiments were conducted under vacuum conditions of approximately 10^{-5} Torr, corresponding to near-Earth space vacuum levels. To evaluate the thrust characteristics of the PPT, the ballistic-pendulum method was used. This approach is widely applied for diagnosing small impulse bits (1–50 μN·s) and provides high accuracy under the short discharge-pulse conditions typical for PPTs [15].

The experimental setup consisted of a lightweight pendulum with a known mass mounted on a thin thread of fixed length (Figure 1a). The plasma pulse generated by the discharge between the planar graphite electrodes produced a short mechanical impulse that caused the pendulum to deflect by a certain angle. The process was recorded with a conventional video camera, followed by frame-by-frame analysis, which enabled determination of the displacement amplitude with an accuracy of no worse than 0.1 mm.

The thrust impulse I_{bit} was calculated using the classical ballistic-pendulum expression:

$$I_{bit} = m\sqrt{2 \times g \times \left(L - \sqrt{L^2 - x^2}\right)}. \quad (1)$$

where m is the pendulum mass, L is the string length, x is the maximum lateral displacement, g is the gravitational acceleration.

The applicability of this method is justified by preliminary analysis: the discharge-pulse duration in the system is on the order of several microseconds, which is significantly shorter than the natural oscillation period of the pendulum. Therefore, the effect of the plasma jet can be treated as an impulse action.

3. Results and Discussion

3.1. Discharge Current Measurement

An example of discharge-current oscillograms at various charging voltages of the main capacitor (from 800 to 1400 V) at a fixed capacitance of C = 4.5 μF is shown in Figure 2. The maximum discharge current reached 3.16 kA at a voltage of 1.4 kV, while the pulse waveform preserved a stable oscillatory structure with gradual damping. The oscillatory shape of the pulse indicates the behavior of an LC discharge in a low-inductance system; the duration of the first half-cycle is approximately 1.1 μs, which corresponds to the formation and ejection time of the plasma sheet within the interelectrode gap.

The power oscillogram shown in Figure 3 was obtained by point multiplication of current and voltage.

In the time interval $t \approx 0 - 0.75$ μs, a sharp change in power is observed, indicating a rapid release of energy in the form of electrical power caused by trigger breakdown. At this moment, an ionized conductive channel was formed, accompanied by a sharp rise in current under high voltage. A numerical calculation of the area under the instantaneous power curve was performed in the range from 0 to 0.75 μs (indicated by the arrowed line on the graph). As a result of the integration, the energy transferred to the load in the form

of a current pulse through the plasma channel was determined to be $E_d = 0.48$ J. At the same time, the initial energy E_c stored in the capacitor is as follows:

$$E_c = \frac{CU^2}{2} = 4.1 \text{ J}. \quad (2)$$

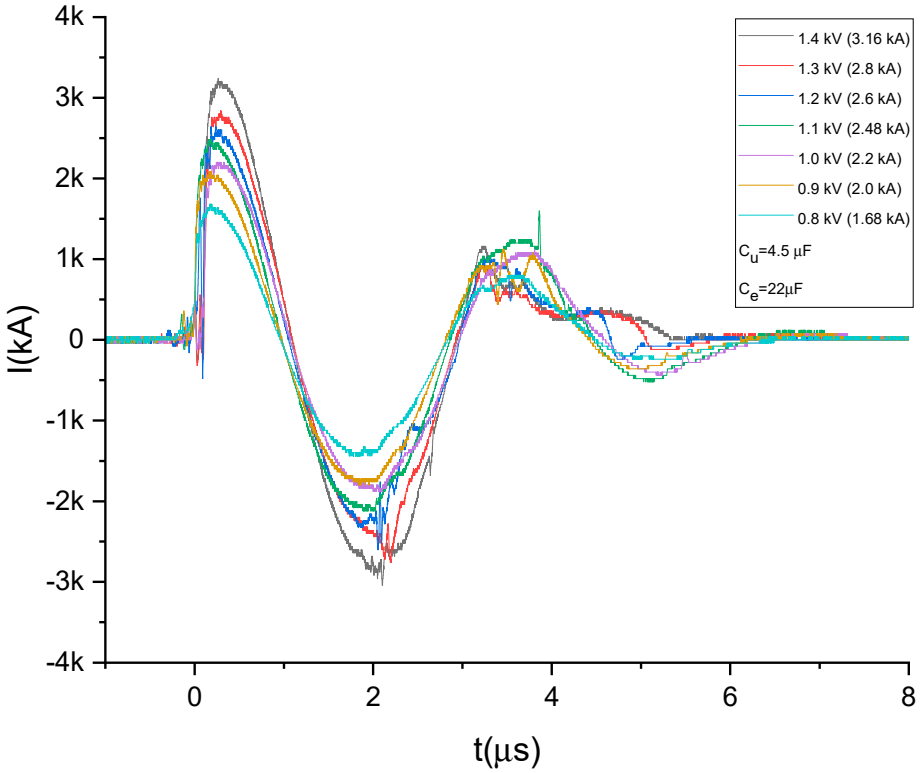


Figure 2. Discharge-current oscillograms at different discharge-energy levels.

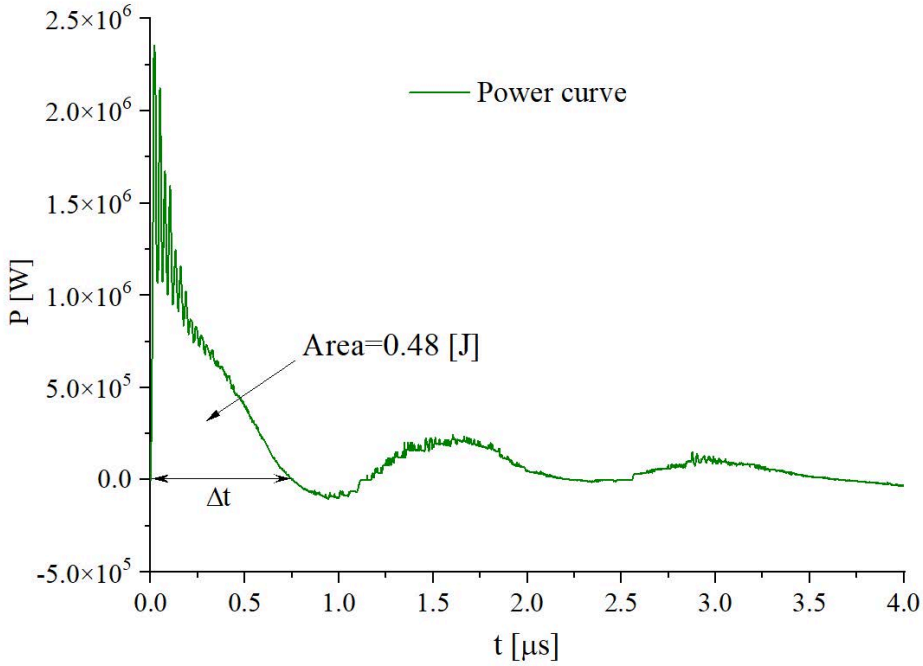


Figure 3. Oscillogram of the discharge power.

Energy transfer efficiency:

$$\eta = \frac{E_d}{E_c} \times 100\% \approx 11.7\%. \quad (3)$$

A major advantage of solid-state plasma thrusters is their simple design and the possibility of miniaturization. However, the available data indicate that the efficiency of such compact engines is on the order of 10% [14,16–19].

3.2. Spectral Analysis

The elemental composition of the plasma jet was examined using spectral analysis with a broadband spectrometer featuring a resolution of 0.1 nm. One representative spectrum is shown in Figure 4, where distinct emission lines of neutral carbon (CI) are clearly identified at wavelengths 427.294, 515.6, 521.79, 656.492, 657.8, and 723.59 nm, indicating the active contribution of the graphite electrode to the formation of the propellant plasma.

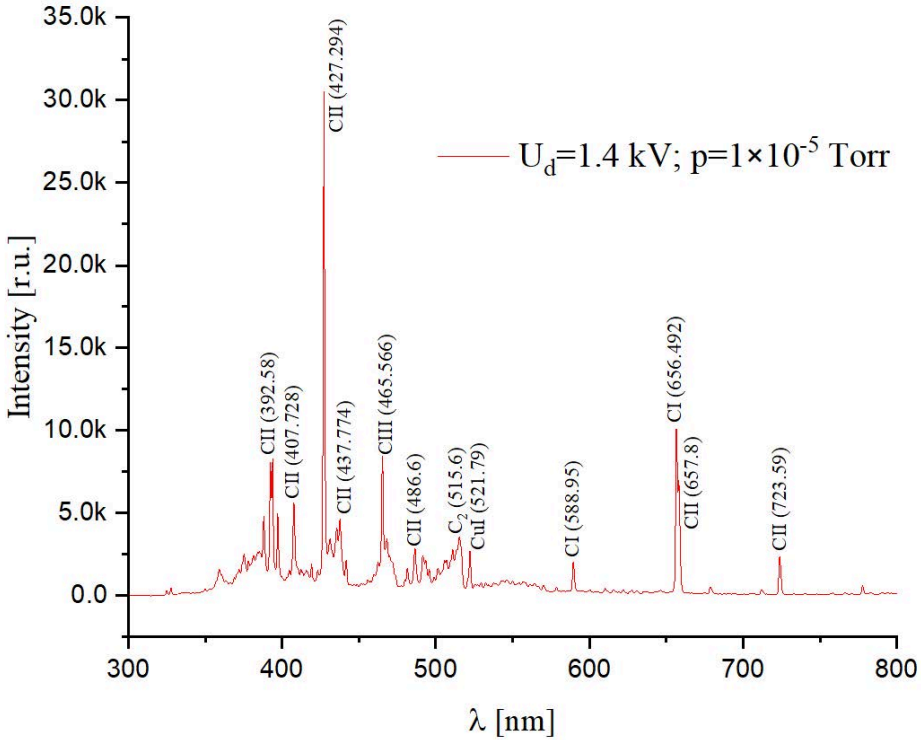


Figure 4. Emission spectrum of the PPT plasma jet. The spectrum was obtained using an Optosky ATL30007 spectrometer manufactured by Optosky Technology Co., Ltd. in Xiamen, China, and the spectral lines were identified with reference to the NIST Atomic Spectra Database.

The formed plasma channel contains predominantly copper ions (Cu^+), carbon ions (C^+), as well as electrons and neutral atoms. Interpretation of the spectrum shows that carbon is the dominant plasma component, appearing in both neutral (CI) and ionized (CII, CIII) states. This is a consequence of using the graphite igniting electrode, which simultaneously serves as the solid propellant. Analysis of the relative intensities of CI and CII lines shows that most of the carbon remains in the neutral state, which is characteristic of APPTs operating at moderate plasma temperatures. When the triggering graphite electrode comes into contact with the copper cathode, erosion occurs not only in the graphite, which provides propellant injection into the interelectrode gap, but also in the cathode itself. The presence of Cu I spectral lines at 521.79 nm indicates erosion of the copper electrodes under pulsed-discharge exposure. This effect is undesirable, as it leads to degradation of the

cathode surface and reduced reproducibility of the discharge characteristics. In the present study, this issue is not addressed in detail and requires a dedicated investigation.

Nevertheless, several potential approaches to mitigating this effect can be identified, in particular the use of a copper cathode with a tungsten insert. Such an insert consists of a small tungsten pellet integrated into the cathode at the contact region with the graphite electrode. Under the considered operating conditions, tungsten is practically resistant to electroerosion at spark-discharge currents and the corresponding temperatures in the electrical contact region, as demonstrated in our previous studies [11]. The use of this cathode configuration can therefore be regarded as a promising approach to improving electrode lifetime and enhancing thruster operational stability.

3.3. High-Speed Imaging and Plasma-Jet Dynamics

Processing of the high-speed video recordings made it possible to reconstruct the spatiotemporal evolution of the discharge in the interelectrode gap of the planar-parallel configuration. Numerous experiments were carried out; one representative example is shown in Figure 5, illustrating the temporal evolution of the plasma formation between the planar electrodes of the PPT.

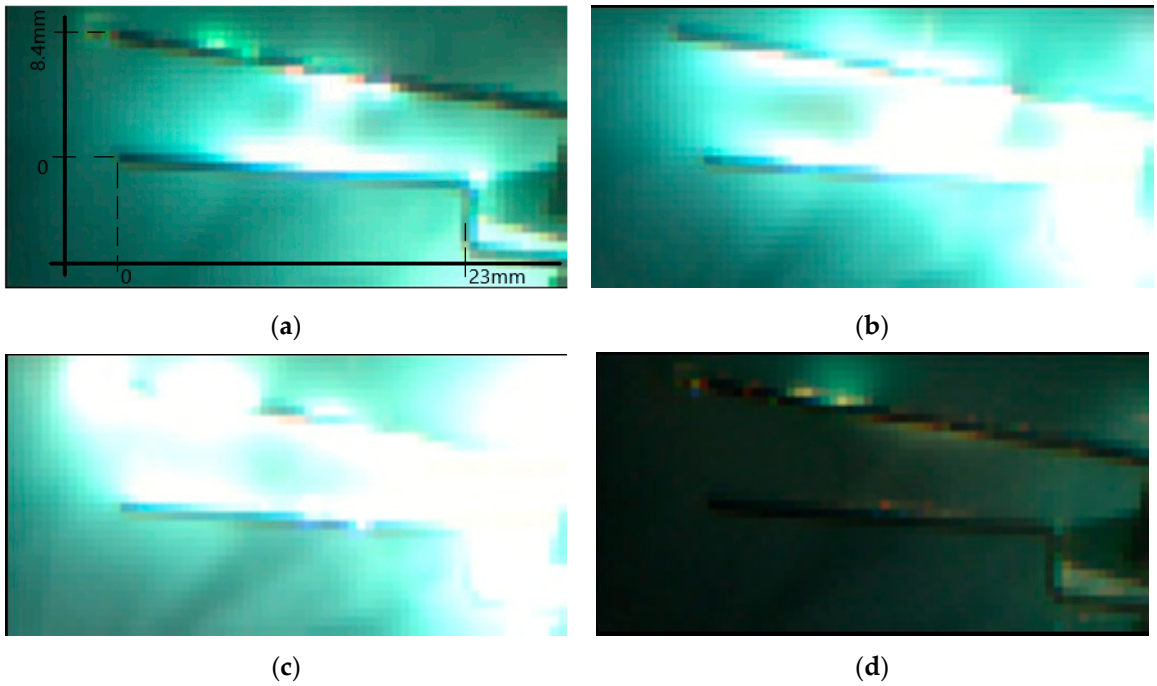


Figure 5. High-speed camera frames illustrating the evolution of the plasma jet. (**a**) 1.41 μs, (**b**) 2.82 μs, (**c**) 4.23 μs, (**d**) 6.64 μs.

The high-speed frames (Figure 5) clearly reveal three stages of discharge development in the planar geometry. At the initiation stage, a local breakdown occurs: the spark ignition generates seed electrons, microparticles, and dust fragments of the graphite material, a significant portion of which becomes partially ionized at the moment of formation. This produces a narrow current channel between the planar electrodes (Figure 5a). This primary channel provides the initial ionization of particles ejected from the igniting graphite electrode and marks the onset of plasma-channel formation. At this stage, erosion processes on the cathode may also contribute: the released propellant material and the local pressure of the current channel can induce additional erosion of the cathode surface. This is supported by the presence of copper emission lines in the plasma spectrum (see Figure 5). The corresponding mechanism is described in detail in [20].

The next stage involves the expansion of the channel and the growth of the plasma structure (Figure 5b), which begins to occupy a significant fraction of the interelectrode volume. In a planar configuration, such structures typically form a relatively wide yet thin plasma sheet propagating from the rear of the gap toward the electrode exit [21]. In the active discharge zone, the plasma exhibits high particle energies (Figure 5b,c). Estimated parameters indicate energetic conditions where the mean kinetic energies of electrons and ions correspond to approximately 10^4–10^5 K. Here, the key factor is not the absolute value of the "temperature," but the pronounced nonequilibrium state of the plasma within the current channel. The system consists of a mixture of neutral particles, ions, and electrons with high current density and significant local pressure gradients, which govern the plasma-acceleration mechanisms [3,20].

Plasma acceleration is defined by three interrelated processes. First, a substantial contribution arises from the dynamic pressure of the ejected particles, which include both heated neutral atoms and ions produced during the spark breakdown. For ablative PPTs, material-ablation processes of the propellant play a key role in this mechanism [22]. Secondly, the thermal expansion of the plasma arising from the local heating of the thin near-electrode layer leads to strong pressure gradients and axial expansion, which is converted into a directed flow in the presence of an exit channel; this mechanism is identified as one of the fundamental processes in classical PPT studies [3]. Thirdly, when a dense current sheet is formed, its self-generated magnetic field interacts with the discharge current, producing a Lorentz force that drives electromagnetic acceleration of the plasma layer; for pulsed ablative accelerators, the J×B contribution becomes dominant at sufficiently high current density, enabling the attainment of high exhaust velocities [21,23].

It should be noted that under real operating conditions all three mechanisms act simultaneously, and their relative importance depends on the discharge energy, electrode geometry and area, as well as the vacuum conditions. In a planar–parallel configuration, the absence of radial symmetry leads to partial energy dissipation through lateral plasma leakage and thermal losses; this results in a more fragmented, multi-jet plume structure compared to coaxial systems, which is consistent with experimental data on modified planar PPTs [21]. At the final stage, the plasma layer detaches from the interelectrode gap and propagates into free space, forming a directed pulsed jet and generating reactive thrust, which is supported by observations of cloud dynamics in studies of ablative plume visualization (Figure 5d).

The velocity of the plasma-plume front was determined from consecutive frames of high-speed imaging. With an interframe interval of 1.41 μs, the displacement of the bright plasma front was measured from the interelectrode region to the exit zone beyond the electrodes. Based on the video-data processing, the average plasma-jet velocity was found to be 11–11.5 km/s, which corresponds to typical values for PPTs and agrees with previously published PPT data [2,11].

3.4. Impulse-Bit Measurements Using a Ballistic Pendulum

To determine the thrust characteristics of PPTs, various pendulum-based thrust stands are widely used, including suspended (translational) ballistic pendulums [19,24,25]. The main advantages of suspended pendulum systems include their simple mechanical design, the ability to rapidly obtain experimental data with acceptable first-order accuracy, and high system stability ensured by gravity acting as a restoring force.

When a horizontal impulse force F is applied, a pendulum with suspension length L is deflected by an angle θ. Under the small-angle approximation ($\theta \ll 1$), the following relationship holds: $F \approx m\,g\theta$. The corresponding linear displacement of the target is given by $x \approx L\theta \approx \frac{L}{m\,g}F$. Thus, the static sens itivity of the pendulum is determined solely by

the pendulum mass and the suspension length. Increasing the ratio L/m enhances the measurement resolution; however, excessively large values lead to increased influence of parasitic forces and reduced system stability. Therefore, in practice, a compromise value is selected to ensure linearity and an acceptable noise level within the operating impulse range.

The impulse bit (I_{bit}) is determined from the potential energy gained by the pendulum during its deflection [19]:

$$I_{bit} = F\Delta t = m\sqrt{2 \times g \times \left(L - \sqrt{L^2 - x^2}\right)}, \tag{4}$$

where m is the pendulum mass, L is the suspension length, x is the maximum lateral displacement, and g is the gravitational acceleration.

The pendulum sensitivity according to Equation (1) can be expressed as

$$h(x) = L - \sqrt{L^2 - x^2} \tag{5}$$

and therefore

$$I_{bit} = m\sqrt{2gh}$$

Taking the derivative yields

$$\frac{dI}{dx} = m\frac{g}{\sqrt{2gh(x)}} \times \frac{x}{\sqrt{L^2 - x^2}}, \tag{6}$$

which represents the exact sensitivity of the ballistic pendulum at any displacement x. This sensitivity is not constant; nonlinear effects increase at larger deflections.

In practice, the sensitivity is often evaluated in the linear approximation assuming $x \ll L$, for which

$$L - \sqrt{L^2 - x^2} \approx \frac{x^2}{2L} \tag{7}$$

Substituting into the impulse expression gives

$$I_{bit} = m\sqrt{2g\frac{x^2}{2L}} = mx\sqrt{\frac{g}{L}} \approx \left(m\sqrt{\frac{g}{L}}\right) \times x \tag{8}$$

Hence, the constant linear sensitivity is

$$\frac{dI}{dx} \approx m\sqrt{\frac{g}{L}} \tag{9}$$

Equation (8) is particularly convenient, as it yields a direct proportionality between impulse bit and displacement within the small-deflection operating range.

For suspended ballistic pendulums, linearity is typically defined by the small-angle condition

$$tan\theta \approx \theta\ [rad], \quad x \approx L\theta \tag{10}$$

i.e., $\frac{x}{L} \ll 1$. Practical criteria are as follows:

- Strictly linear: $\frac{x}{L} \leq 1$ (error due to $tan\theta \approx \theta \sim 0.3\%$).
- Acceptably linear: $\frac{x}{L} \leq 0.2$ (error of about 1–1.5%).

In the present experiments, a ballistic pendulum with the following parameters was used: $m = 1.7{\cdot}10^{-4}$ kg; $L = 6.15{\cdot}10^{-4}$ m.

The static sensitivity of the pendulum under these conditions, within the linear approximation, is

$$\frac{dI}{dx} = 2.15\ \mu\text{N}\cdot\text{s/mm} \tag{11}$$

The relative error can be estimated as $\varepsilon \sim \frac{\theta^2}{3}$. Assuming a linearity criterion of 5% corresponds to $\theta \approx 0.3$. The maximum allowable displacement is then $x_{max} = 30.75$ mm, which corresponds to a maximum impulse bit of

$$I_{bit\ max} \approx 2.15 \cdot x_{max} \approx 68.35\ \mu\text{N}\cdot\text{s}. \tag{12}$$

Thus, within the impulse-bit range of 0–68 μN ·s, the pendulum response can be considered linear with an error not exceeding 5%, which is more than sufficient for first-order experimental investigations.

The maximum measured impulse bit reached approximately 17.1 μN ·s, which corresponds to a pendulum displacement of 7.97 mm. This value is consistent with the plasma exhaust velocities obtained from high-speed imaging. Based on the measured impulse-bit values, the specific impulse at a discharge voltage of 1400 V was estimated to be in the range of 1000–1200 s, confirming the effectiveness of graphite propellant in this discharge-channel configuration [21]. Table 2 summarizes the impulse-bit values for different capacitor-stored energies. The methods for calculating the thrust and energy characteristics are described in detail in our previous works [11].

Table 2. Impulse bit at various discharge energies.

U, kV	W, J	I, kA	I, μN·s
1.4	4.41	3.16	17.1
1.3	3.80	2.8	16
1.2	3.24	2.6	15.3
1.1	2.72	2.48	14.3
1.0	2.25	2.2	12.7

The combination of these parameters makes this type of thruster suitable for a wide range of space-maneuvering applications [17]:

- Orbit correction and attitude control;
- Satellite deorbiting;
- Formation of satellite constellations (swarming/formation flying);
- Maneuvering of SSC near objects, including inspection missions [26].

A promising direction for further development is the creation of cassette-type systems based on multiple PPT modules, aimed at increasing the total thrust or enabling vector control [27]. The design can also be scaled for use with higher-capacity power supplies or solar-energy storage systems, enabling applications on medium-class spacecraft [28].

In general, the impulse bit increases with increasing discharge energy. The magnitude of the impulse bit is determined by the discharge current, which in turn depends on the energy stored in the capacitor bank. Table 3 presents a comparison of the thrust characteristics obtained in the present study with results reported by other authors investigating planar ablative plasma thrusters.

Table 3. Comparison of thrust characteristics with results reported by other authors.

W [J]	I_{bit} [μN·s]	References to Related Works
2.25–4.41	12.7–17.1	This work
2–4	15–30	[29]
2.25	22.4–39.1	[30]
8	~38 (50)	[31]

As shown in Table 3, the laboratory prototype of the planar-electrode plasma thruster investigated in this work exhibits lower thrust performance compared to several previously reported ablative thrusters. However, these results should not be regarded as limiting. Further optimization of the thruster design and discharge regimes represents a promising pathway for increasing the impulse bit. On the other hand, relatively low impulse-bit values can be compensated by increasing the number of operating pulses, provided that the operational characteristics and durability of the thruster are improved.

A key advantage of the proposed configuration compared with conventional ablative thrusters is the ignition system, which enables the use of various electrically conductive materials as propellants. This feature significantly broadens the potential for further optimization and improvement of the plasma thruster's key performance characteristics.

Compared with our previously developed PPTs, which were implemented in a coaxial configuration, the proposed planar PPT demonstrates clear design and research-related advantages [10,11]. From an engineering standpoint, the planar geometry is structurally simpler and requires significantly less material, resulting in a reduced overall mass compared to coaxial designs, which inherently involve a larger electrode volume. In addition, the planar configuration provides improved accessibility of the discharge region, making it more convenient for experimental diagnostics and systematic investigation of plasma acceleration and ablation processes [32]. Despite the substantial reduction in mass and structural complexity, the thrust performance of the planar thruster remains comparable to that of the earlier coaxial prototypes.

Thus, the developed PPT represents an accessible, technologically simple, and potentially mass-producible solution for electrodynamic maneuvering in low-Earth orbit and near-planet environments.

4. Conclusions

The present work introduces the design and experimental characterization of a solid-propellant PPT employing graphite as both the ablation propellant and ignition element. The proposed configuration is based on a plane–parallel acceleration channel equipped with an electromagnetic initiation mechanism that provides controlled contact between the igniter electrode and the cathode. The experiments confirmed stable thruster operation under a vacuum of 10^{-5} Torr, reliable discharge formation at voltages of 800–1400 V, and high repeatability of pulses over multiple firing sequences. The peak discharge current reached 3.16 kA, with the energy per pulse up to 4.41 J. Spectral analysis verified the active contribution of graphite to plasma formation, while high-speed imaging revealed the development of a narrow and stable plasma jet with a characteristic exhaust velocity of up to 11.5 km/s. The measured thruster efficiency of approximately 11.7% represents a strong performance indicator for pulsed plasma systems and confirms the effectiveness of the developed architecture and the adequacy of the chosen design parameters.

The thruster is distinguished by its structural simplicity, a small number of components, the absence of complex moving parts, and the use of readily available materials. These features make it promising for integration into SSCsystems, particularly for orbit maneuvering, attitude control, and proximity operations. Future work will include test-

ing over a broader range of operating parameters, alongside the parallel development of a multi-module cassette configuration aimed at increasing total thrust and extending operational lifetime.

5. Patents

The patent "Pulsed Plasma Thruster on Graphite Propellant for Nanosatellites" (Kazakhstan Patent No. 2025/0433.2) has been granted.

Author Contributions: Conceptualization and writing—original draft preparation: M.D. and Z.I.; methodology: Z.I. and O.Y.; supervision: M.D.; data curation: M.D., Z.I. and O.Y.; writing—review and editing supported by M.D. and Z.I.; funding acquisition: M.D. All authors have read and agreed to the published version of the manuscript.

Funding: This research was funded by the Committee of Science of the Ministry of Science and Higher Education of the Republic of Kazakhstan (Grant No. AP32727031 & Grant No. AP19576858).

Data Availability Statement: The original contributions presented in the study are included in the article: further inquiries can be directed to the corresponding author.

Conflicts of Interest: The authors declare no conflicts of interest.

References

1. Ling, W.Y.L.; Zhang, S.; Fu, H.; Huang, M.; Quansah, J.; Liu, X.; Wang, N. A Brief Review of Alternative Propellants and Requirements for Pulsed Plasma Thrusters in Micropropulsion Applications. *Chin. J. Aeronaut.* **2020**, *33*, 2999–3010. [CrossRef]
2. Wagner, H.P.; Auweter-Kurtz, M. Pulsed Plasma Thrusters for Space Propulsion and Industrial Processing. In Proceedings of the 28th International Electric Propulsion Conference, Toulouse, France, 17–21 March 2003.
3. Chan, Y.-A.; Montag, C.; Herdrich, G.; Schönherr, T. Review of Thermal Pulsed Plasma Thruster-Design, Characterization, and Application. In Proceedings of the 34th International Electric Propulsion Conference, Kobe-Hyogo, Japan, 4–10 July 2015.
4. Jakubczak, M.; Riazantsev, A.; Cichorek, O.; Jardin, A.; Kurzyna, J.; Drożdż, P.; Palacz, T.; Chuchla, M.; Łabuz, R.; Bywalec, G. Design and Performance of a 1 J Ablative Pulsed Plasma Thruster Fed with Non-Volatile Liquid Propellant. *Acta Astronaut.* **2025**, *228*, 813–827. [CrossRef]
5. Keidar, M. Micro-Cathode Arc Thruster for Small Satellite Propulsion. In Proceedings of the 2016 IEEE Aerospace Conference, Big Sky, MT, USA, 5–12 March 2016; pp. 1–7.
6. Zhang, Z.; Schäfer, F.; Zhang, G.; Tang, H.; Ling, W.Y.L.; Herdrich, G.; York, T.M. Investigation on Operational Stability of a Pulsed Plasma Thruster with a Pressure Probe. *Acta Astronaut.* **2022**, *197*, 60–68. [CrossRef]
7. Yang, L.; Liu, X.; Guo, W.; Wu, Z.; Wang, N. Simulation of Parallel-Plate Pulsed Plasma Teflon® Thruster Based on the Electromechanical Model. In Proceedings of the 2010 2nd International Conference on Advanced Computer Control, Shenyang, China, 27–29 March 2010; pp. 148–151.
8. Ashraf, A.; Yaqub, K.; Javeed, S.; Zeeshan, S.; Khalid, R.; Janjua, S.; Ahmad, S. Sublimation of Graphite in Continuous and Pulsed Arc Discharges. *Turk. J. Phys.* **2010**, *34*, 33–42. [CrossRef]
9. O'Reilly, D.; Herdrich, G.; Schäfer, F.; Montag, C.; Worden, S.P.; Meaney, P.; Kavanagh, D.F. A Coaxial Pulsed Plasma Thruster Model with Efficient Flyback Converter Approaches for Small Satellites. *Aerospace* **2023**, *10*, 540. [CrossRef]
10. Dosbolayev, M.K.; Igibayev, Z.B.; Tazhen, A.B.; Ramazanov, T.S. Preliminary Study of the Solid-State Pulsed Plasma Thruster Model with Graphite as a Propellant. *Plasma Phys. Rep.* **2022**, *48*, 263–270. [CrossRef]
11. Dosbolayev, M.; Igibayev, Z.; Ussenov, Y.; Suleimenova, A.; Aldabergenova, T. Study of the Design and Characteristics of a Modified Pulsed Plasma Thruster with Graphite and Tungsten Trigger Electrodes. *Appl. Sci.* **2025**, *15*, 10767. [CrossRef]
12. Keidar, M.; Boyd, I.D.; Beilis, I.I. Model of an Electrothermal Pulsed Plasma Thruster. *J. Propuls. Power* **2003**, *19*, 424–430. [CrossRef]
13. Burton, R.L.; Turchi, P.J. Pulsed Plasma Thruster. *J. Propuls. Power* **1998**, *14*, 716–735. [CrossRef]
14. Zhang, Z.; Ling, W.Y.L.; Tang, H.; Cao, J.; Liu, X.; Wang, N. A Review of the Characterization and Optimization of Ablative Pulsed Plasma Thrusters. *Rev. Mod. Plasma Phys.* **2019**, *3*, 5. [CrossRef]
15. Aheieva, K.; Toyoda, K.; Cho, M. Vacuum Arc Thruster Development and Testing for Micro and Nano Satellites. *Aerosp. Technol. Jpn.* **2016**, *14*, Pb_91–Pb_97. [CrossRef]
16. Riazantsev, A.; Jakubczak, M.; Cichorek, O.; Kurzyna, J. Side and Front Fast Imaging of Solid and Liquid Fed Ablative Pulsed Plasma Thruster's Discharge. *Acta Astronaut.* **2024**, *225*, 583–594. [CrossRef]

17. Ou, Y.; Wu, J.; Cheng, Y.; Zhang, Y.; Che, B. Design and Performance of a Micro-Pulsed Plasma Thruster Used in Miniaturized Satellites. *Adv. Space Res.* **2024**, *74*, 1741–1750. [CrossRef]
18. Lee, H.C.; Lim, C.H.; Woo, H.J.; Goh, B.T.; Chin, O.H.; Tou, T.Y. Performance of Pulsed Plasma Thruster at Low Discharge Energy. *Plasma Sci. Technol.* **2024**, *26*, 045502. [CrossRef]
19. Aheieva, K.; Fuchikami, S.; Nakamoto, M.; Toyoda, K.; Cho, M. Development of a Direct Drive Vacuum Arc Thruster Passively Ignited for Nanosatellite. *IEEE Trans. Plasma Sci.* **2016**, *44*, 100–106. [CrossRef]
20. Shaw, P.; Lappas, V.J. Modeling of a Pulsed Plasma Thruster; Simple Design, Complex Matter. In Proceedings of the In Space Propulsion Conference, San Sebastian, Spain, 3–6 May 2010.
21. Schönherr, T.; Nees, F.; Arakawa, Y.; Komurasaki, K.; Herdrich, G. Characteristics of Plasma Properties in an Ablative Pulsed Plasma Thruster. *Phys. Plasmas* **2013**, *20*, 033503. [CrossRef]
22. Zeng, L.; Wu, Z.; Sun, G.; Huang, T.; Xie, K.; Wang, N. A New Ablation Model for Ablative Pulsed Plasma Thrusters. *Acta Astronaut.* **2019**, *160*, 317–322. [CrossRef]
23. Thio, Y.C.; Cassibry, J.T.; Markusic, T.E. Pulsed Electromagnetic Acceleration of Plasmas. In Proceedings of the 38th AIAA/ASME/SAE/ASEE Joint Propulsion Conference & Exhibi, Indianapolis, IN, USA, 7–10 July 2002; Available online: https://ntrs.nasa.gov/api/citations/20030002753/downloads/20030002753.pdf (accessed on 5 January 2026).
24. Li, H.; Wu, Z.; Sun, G.; Zhu, K.; Huang, T.; Liu, X.; Ling, W.Y.L.; Wang, N. A Model for Macro-Performances Applied to Low Power Coaxial Pulsed Plasma Thrusters. *Acta Astronaut.* **2020**, *170*, 154–162. [CrossRef]
25. Zhang, H.; Li, D.T.; He, F.; Chen, X.W. Development of an Indirect Thrust Stand Based on a Cantilever Beam. *AIP Adv.* **2021**, *11*, 035006. [CrossRef]
26. Aoyagi, J.; Yamada, M.; Tezuka, T.; Watanabe, R.; Otsuki, T.; Takeya, S. Series Development of Coaxial Pulsed Plasma Thruster from 1 J to 8 J. *J. Electr. Propuls.* **2025**, *4*, 38. [CrossRef]
27. Baek, S.; Kim, H. Research and Development Trends of Pulsed Plasma Thruster for Small Satellites. *J. Korean Soc. Propuls. Eng.* **2025**, *29*, 11–25. [CrossRef]
28. Myers, R.; Oleson, S.; McGuire, M.; Meckel, N.; Cassady, R. Pulsed Plasma Thruster Technology for Small Satellite Missions. In Proceedings of the Annual Small Satellite Conference, Logan, UT, USA, 18–21 September 1995.
29. Li, Y.-H.; Palagiri, S.; Chang, P.-Y.; Montag, C.; Herdrich, G. Plasma Behavior in a Solid-Fed Pulsed Plasma Thruster. *J. Aeronaut. Astronaut. Aviat.* **2019**, *51*, 31–42. [CrossRef]
30. Tran, Q.; Lim, W.; Bui, T.; Kang, B. Development of a Dual-Axis Pulsed Plasma Thruster for Nanosatellite Applications. *J. Small Satell.* **2019**, *8*, 837–847.
31. Miyagi, K.; Kakami, A.; Tachibana, T. Characterization of a Liquid-Propellant Pulsed Plasma Thruster Using Various Nozzle Configurations. *Trans. Jpn. Soc. Aeronaut. Space Sci.* **2019**, *62*, 184–191. [CrossRef]
32. Schönherr, T.; Nawaz, A.; Lau, M.; Petkow, D.; Herdrich, G. Review of Pulsed Plasma Thruster Development at IRS. *Trans. Jpn. Soc. Aeronaut. Space Sci. Aerosp. Technol. Jpn.* **2010**, *8*, Tb_11–Tb_16. [CrossRef]

Disclaimer/Publisher's Note: The statements, opinions and data contained in all publications are solely those of the individual author(s) and contributor(s) and not of MDPI and/or the editor(s). MDPI and/or the editor(s) disclaim responsibility for any injury to people or property resulting from any ideas, methods, instructions or products referred to in the content.